HHS Public Access

Author manuscript

J Magn Reson Imaging. Author manuscript; available in PMC 2021 January 27.

Published in final edited form as:

J Magn Reson Imaging. 2020 February ; 51(2): 580–592. doi:10.1002/jmri.26849.

Evaluation of a Motion-robust 2D Chemical Shift-Encoded Technique for R2* and Field Map Quantification in Ferumoxytol-Enhanced MRI of the Placenta in Pregnant Rhesus Macaques

Ante Zhu, MS[1,2], **Scott B. Reeder, MD, PhD**[1,2,3,4,5], **Kevin M. Johnson, PhD**[2,3], **Sydney Nguyen, BS**[6,7], **Thaddeus G. Golos, PhD**[6,7,8], **Ann Shimakawa, MS**[9], **Matthias R Muhler**[2], **Christopher J. Francios**[2], **Ian M. Bird, PhD**[8], **Sean B. Fain, PhD**[1,2,3], **Dinesh M. Shah, MD**[7], **Oliver Wieben, PhD**[2,3], **Diego Hernando, PhD**[1,2,3,10]

[1.]Department of Biomedical Engineering, University of Wisconsin, Madison, Wisconsin, USA

[2.]Department of Radiology, University of Wisconsin, Madison, Wisconsin, USA

[3.]Department of Medical Physics, University of Wisconsin, Madison, Wisconsin, USA

[4.]Department of Medicine, University of Wisconsin, Madison, Wisconsin, USA

[5.]Department of Emergency Medicine, University of Wisconsin, Madison, Wisconsin, USA

[6.]Wisconsin National Primate Research Center, University of Wisconsin, Madison, Wisconsin, USA

[7.]Department of Obstetrics and Gynecology, University of Wisconsin, Madison, Wisconsin, USA

[8.]Department of Comparative Biosciences, University of Wisconsin, Madison, Wisconsin, USA

[9.]Global MR Applications and Workflow, GE Healthcare, Menlo Park, California, USA

[10.]Department of Electrical and Computer Engineering, University of Wisconsin, Madison, Wisconsin, USA

Abstract

Background: 3D chemical shift-encoded (CSE)-MRI techniques enable assessment of ferumoxytol concentration but are unreliable in the presence of motion.

Purpose: To evaluate a motion-robust 2D-sequential CSE-MRI for R2* and B0 mapping in ferumoxytol-enhanced MRI of the placenta.

Study Type: Prospective.

Animal Model: Pregnant rhesus macaques.

Field Strength/Sequence: 3.0T/CSE-MRI.

Assessment: 2D-sequential CSE-MRI was compared with 3D respiratory-gated CSE-MRI in placental imaging of eleven anesthetized animals at multiple time points before and after

Correspondence to: Diego Hernando, Departments of Radiology and Medical Physics, University of Wisconsin. WIMR 2474, 1111 Highland Ave., Madison, WI, USA, 53792. dhernando@wisc.edu. Tel: 1-608-265-7590.

ferumoxytol administration, and in ferumoxytol phantoms (0μg/mL-440μg/mL). Motion artifacts of CSE-MRI in ten pregnant women without ferumoxytol administration were assessed retrospectively by three blinded readers (4-point Likert scale). The repeatability of CSE-MRI in seven pregnant women was also prospectively studied.

Statistical Tests: Placental R2* and boundary B0 field measurements (ΔB0) were compared between 2D-sequential and 3D respiratory-gated CSE-MRI using linear regression and Bland-Altman analysis.

Results: In phantoms, a slope of 0.94 (r^2=0.99, concordance correlation coefficient ρ=0.99) and bias of $-4.8s^{-1}$ (limit of agreement-LOA, $-41.4s^{-1}$, $+31.8s^{-1}$) in R2*, and a slope of 1.07 (r^2=1.00, ρ=0.99) and bias of 11.4Hz (LOA −12.0Hz, +34.8Hz) in ΔB0 were obtained in 2D CSE-MRI compared to 3D CSE-MRI for reference R2*≤$390s^{-1}$. In animals, a slope of 0.92 (r^2=0.97, ρ=0.98) and bias of $-2.2s^{-1}$ (LOA $-55.6s^{-1}$, $+51.3s^{-1}$) in R2*, and a slope of 1.05 (r^2=0.95, ρ=0.97) and bias of 0.4Hz (LOA −9.0Hz, +9.7Hz) in ΔB0 were obtained. In humans, motion impaired R2* maps in 3D CSE-MRI (Reader-1: 1.8±0.6, Reader-2: 1.3±0.7, Redaer-3: 1.9±0.6), while 2D CSE-MRI was motion-free (Reader-1: 2.9±0.3, Reader-2: 3.0±0, Reader-3: 3.0±0). A mean difference of $0.66s^{-1}$ and coefficient of repeatability of $9.48s^{-1}$ for placental R2* were observed in the repeated 2D CSE-MRI.

Data Conclusion: 2D-sequential CSE-MRI provides accurate R2* and B0 measurements in ferumoxytol-enhanced placental MRI of animals in the presence of respiratory motion, and motion-robustness in human placental imaging.

Keywords

placenta; ferumoxytol; chemical shift-encoded; R2*; B0 field; motion-robust

Introduction

In the pathologies of preeclampsia, an inflammatory condition of pregnancy that can lead to edema, hypertension, seizures and even death, altered immune cell (e.g. macrophage) activation and distribution at the implantation site may play an important role (1). The FDA-approved iron supplement ferumoxytol is an ultra-small superparamagnetic iron oxide nanoparticle (SPION) which is transported in blood after intravenous infusion (2), accumulates in organs like the liver and spleen, and is phagocytosed by activated macrophages over a period of days. Ferumoxytol leads to increases in R1 and R2* relaxation rates, and its magnetic susceptibility effects can also be quantified through B0 field measurement-based techniques.

A previously proposed 3D chemical shift-encoded (CSE) MRI method has been demonstrated to enable R2* mapping-based and B0 mapping-based assessment of different iron concentrations in SPION phantoms (3), ferumoxytol-enhanced brain MRI (4, 5) and body iron deposition (3, 6, 7). Therefore, ferumoxytol-enhanced CSE-MRI may enable non-invasive and sensitive detection of increased macrophage density in inflammation at the maternal-fetal interface, similar to what has been shown in other investigations including inflammation of the central nervous system, aortic walls, kidneys, pancreas and others (8, 9).

Maternal respiratory and fetal motion in the uterus are challenges for imaging the placenta with MRI (10) and their effects should be addressed in order to minimize bias and maximize precision in CSE-MRI. Imaging acquisition in a breath-hold has been shown to reduce respiratory motion artifacts in 3D CSE-MRI (11). However, breath-hold requirements may reduce the comfort of pregnant patients and the corresponding scan time constraints may limit the achievable spatial resolution and image signal-to-noise ratio (SNR). Respiratory-gated (12, 13) and free-breathing non-Cartesian acquisition techniques (14, 15) have been applied in body 3D CSE-MRI during free-breathing and shown to be motion robust.

Compared to 3D CSE-MRI which has a long temporal footprint, e.g., a typical scan time of ~5 minutes in respiratory-gated imaging and ~3 minutes in free-breathing imaging (15), 2D CSE-MRI with sequential phase encoding has a short temporal footprint. It enables acquisition of images in a single slice in ~3 seconds (16). This strategy is expected to freeze motion or contain the motion effects to a limited number of slices (17, 18). 2D MRI-based R2* mapping has been applied in the placenta using breath-hold acquisitions (19, 20). Free-breathing 2D CSE-MRI in the liver has been demonstrated to enable accurate measurements on proton density fat fraction (PDFF), an imaging biomarker of fat content that can be quantified simultaneously with R2* and B0 field in CSE-MRI techniques (16). Therefore, free-breathing 2D CSE-MRI may also enable reliable R2* and B0 field measurements in the presence of both maternal respiratory motion and fetal motion. Furthermore, motion-robust R2* mapping using 2D CSE-MRI, as evaluated in this work, may also enable reliable assessment of placental health with endogenous contrast, including blood oxygenation level dependent (BOLD)-based placental functional imaging (21).

However, the accuracy of the free-breathing 2D CSE-MRI technique for quantification of R2* and B0 field in ferumoxytol-enhanced MRI of the placenta has not yet been validated and compared to the standard 3D CSE-MRI. Maternal respiratory motion and fetal motion need to be minimized in 3D CSE-MRI in order to provide a reliable reference of R2* and B0 field measurements. Ferumoxytol-enhanced MRI of the nonhuman primate, who has the most similar placentation and immunology with the human reproductive system (22, 23), would be an important step towards evaluating the feasibility of ferumoxytol-enhanced MRI in human pregnancy. Furthermore, the primate mother is anesthetized during the scan, which also anesthetizes the fetus, thereby minimizing fetal motion. This enables reliable imaging with the standard 3D CSE-MRI using respiratory gating, which further minimizes the effect of maternal respiratory motion. Thus, ferumoxytol-enhanced MRI of the animals under general anesthesia enables in vivo evaluation of the accuracy of 2D CSE-MRI in the presence of maternal respiratory motion, by comparing to the reference 3D respiratory-gated CSE-MRI.

In summary, the purpose of this study was to evaluate the accuracy of 2D CSE-MRI technique for quantification of R2* and B0 field in ferumoxytol-enhanced MRI of the placenta in pregnant rhesus macaques as well as in ferumoxytol phantoms. The secondary purpose was to preliminarily evaluate the motion artifacts and repeatability for placental R2* mapping enabled by 2D CSE-MRI in pregnant women without ferumoxytol administration.

Materials and Methods

Phantoms

A phantom with varying R2* and magnetic susceptibilities was constructed using ferumoxytol (Feraheme, AMAG Pharmaceuticals Inc., Cambridge, MA). Eight cylindrical 40 mL vials (diameter=20 mm) with varying concentrations of ferumoxytol ranging from 0 μg/mL-440 μg/mL, prepared in an agar gel (2% agar weight/volume, 3 mM sodium benzoate, 43 mM NaCl) were built and were separated into two batches, which were scanned sequentially. Four vials in each batch were placed in a holder within a cylindrical plastic container filled with distilled water. Phantoms were placed in the scanner with the long axis of the vials parallel to the main magnetic field. A hemisphere photopolymer resin phantom with the same radius as the cylindrical plastic container was attached to the bottom wall of the cylindrical container to reduce magnetic susceptibility effects at the interface.

Animals

All procedures were approved by our institution's animal care and use committee (IACUC). In this study, 2D CSE-MRI and 3D CSE-MRI acquisitions were obtained and compared in ferumoxytol-enhanced MRI of pregnant rhesus macaques, who normally have two placental discs, one primary large disc and one secondary smaller disc (24). The two discs are attached to the anterior and posterior uterus walls (25), separately, which were named as anterior placental disc and posterior placental disc in this study.

Eleven pregnant rhesus macaque monkeys at their late second trimester based on an average 165 days pregnancy length (gestation age=98.7±5.9, maternal weight=8.8±1.1kg, normal singleton) in a study of inflammation at the maternal-fetal interface[26] were scanned. Each animal was imaged at multiple time points before and after administration of ferumoxytol by intravenous infusion. In each scan session, the animal was anesthetized by administration of up to 10 mg/kg ketamine. Oxygen with 1.5% isoflurane was delivered through inhalation during the scan for prolonged sedation. Ferumoxytol was administered at a dose of 4 mg/kg diluted 5:1 with sterile saline solution. Animals were monitored during and after imaging until fully recovered from anesthesia. Detailed animal information, and details on drug dose and ferumoxytol administration are shown in Supporting Information Table S1.

Humans

Additionally, two preliminary human placental studies, including a motion assessment study and a repeatability study, were performed.

The motion artifacts of 2D CSE-MRI compared to 3D CSE-MRI were preliminarily evaluated in human scans by retrospectively analyzing images in a HIPAA compliant human placental study, approved by the local Institutional Review Board (IRB). Pregnant women with singleton in normal pregnancy were recruited. Exclusion criteria included subjects with any previous pregnancy conditions, including hypertension, preeclampsia, or diabetes. In this study, pregnant women at 20–22 weeks of gestation were scanned after obtaining informed written consent. MR images of ten human subjects were evaluated. Details on the subject information are shown in Supporting Information Table S2.

Further, the repeatability of 2D and 3D CSE-MRI for placental R2* mapping was also preliminarily evaluated in seven pregnant women scans at either 14–15 or 20–22 weeks of gestation in the human placental study above. Details on the subject information are shown in Supporting Information Table S3.

Imaging Protocol

Phantom and animals were imaged using a clinical 3.0T MRI system (GE Healthcare Discovery MR 750, Waukesha, WI) with a 32-channel phased array torso coil (Neocoil, Pewaukee, WI). Pregnant women were imaged using a clinical 1.5T MRI system (GE Healthcare Optima MR450w, Waukesha, WI) without contrast agent administration.

Phantoms—In the phantom study, a multi-echo spoiled gradient-echo (SGRE) 2D acquisition ("2D CSE-MRI") and a multi-echo SGRE 3D acquisition ("3D CSE-MRI") were used. The scan parameters for these 2D and 3D CSE-MRI acquisitions were chosen such that SNR (SNR=35 in 2D CSE-MRI, SNR=60 in 3D CS-MRI) approximately matched that observed in the 2D and 3D CSE-MRI acquisitions, respectively, in the animal study (described below). In addition, a 3D CSE-MRI acquisition with high SNR ("3D CSE-MRI high SNR", SNR=235), obtained by increasing slice thickness, was used as reference for both R2* and B0 field measurements. A second 2D CSE-MRI acquisition with relatively high SNR ("2D CSE-MRI high SNR", SNR=90), obtained by increasing the number of averages, was also performed to assess 2D CSE-MRI while diminishing SNR-related effects on measurements. Details on the acquisition parameters of the four CSE-MRI acquisitions are listed in Table 1.

Animals—In the rhesus study, the animal was placed in the left lateral decubitus position in the MRI scanner. Scans at each time point included an axial 2D CSE-MRI acquisition without respiratory gating, designed for motion-robust ferumoxytol-enhanced CSE-MRI and performed in each animal covering the maternal uterus cavity. An axial 3D CSE-MRI acquisition with respiratory gating using maternal respiratory bellow signals was also acquired as the reference for CSE-MRI in the placenta. Details on the acquisition parameters of the two CSE-MRI acquisitions are listed in Table 1.

Humans—Each subject was scanned in supine position and the field of view was prescribed to cover the maternal uterus cavity. In the motion assessment study, R2* and B0 field mapping were performed from two different acquisitions: an axial 3D CSE-MRI with respiratory gating using maternal respiratory bellow signals, and a free-breathing axial 2D CSE-MRI which was acquired approximately 20 minutes after the 3D CSE-MRI scan. In addition, a 2D multi-slice T2-weighted single-shot fast spin-echo (SSFSE) was acquired for anatomic imaging. Details on the scan parameters are shown in Table 1. In the repeatability study, the 3D respiratory-gated CSE-MRI and the free-breathing 2D CSE-MRI were performed sequentially at the beginning of the exam. The two sequences were repeated 20 minutes afterwards. A 2D multi-slice T2-weighted SSFSE was also acquired.

Imaging Reconstruction, Assessment and Measurements

In all CSE-MRI acquisitions, water-only and fat-only images, R2* and B0 field maps were reconstructed through complex fitting of the multi-echo data using a multi-component signal model (27). In phantom and animals, R2* and boundary B0 measurements were obtained. The boundary B0 field measurement, which measures the difference in the B0 field at both sides of the boundary of two neighboring regions, is directly proportional to the magnetic susceptibility difference between the two regions and has been used as a measure of tissue magnetic susceptibility in previous works (3, 28). A reference for boundary B0 measurements, i.e., a region with approximately constant magnetic susceptibility, was thus used in both phantom and animal studies as described below. In humans, placental R2* measurements were obtained, as described in detail below.

Phantoms—In each of the phantom datasets, co-localized R2* measurements from the 2D and 3D CSE-MRI acquisitions were obtained by placing regions-of-interest (ROIs) over each of the eight vials. Water in the plastic container was used as a reference for boundary B0 measurements. ROIs were drawn in one slice of each vial and the adjacent water, the boundary of which was parallel to the main magnetic field. Measured B0 field values were subtracted to obtain the boundary B0 field difference $\Delta B0=B0_{Vial}-B0_{WaterBath}$. All ROIs were drawn in regions of a homogeneous field to reduce apparent B0 inhomogeneity related bias on measurements.

Animals—In each of the animal datasets, R2* measurements were obtained by drawing six ROIs in the anterior placental disc and six in the posterior placental disc, co-localized in the reconstructed R2* and B0 maps from both 2D and 3D CSE-MRI acquisitions. Three slices with relatively large continuous area of placental tissues in the superior, middle and inferior regions of each placental disc were chosen. Two ~0.6 cm^2 oval ROIs were drawn in two separate areas with relatively large continuous area of placental tissues in each slice. Image quality was assessed independently by three radiologists with 19, 21 and 18 years of experience in radiology (Redear-1: S.R., Reader-2: M.M., Reader-3: C.F., respectively) to either accept R2* map with no significant artifacts and further confirm ROI locations in the placenta, or reject R2* map with severe artifacts. The datasets with both 3D and 2D images accepted by at least two radiologists were used for comparison on R2* and B0 measurements. R2* measurements in 2D versus 3D CSE-MRI were compared in anterior placental disc, posterior placental disc, and in both placental discs together. Amniotic fluid in the uterus was used as a reference for boundary B0 measurements. B0 field values in a ~0.1 cm^2 oval ROI drawn in the placenta and adjacent amniotic fluid, the boundary of which was approximately parallel to the main magnetic field, were measured and subtracted to obtain $\Delta B0=B0_{Placenta}-B0_{AmnioticFluid}$. ΔB0 measurements in 2D versus 3D CSE-MRI were compared in all animals.

Humans—In the motion assessment study, de-identified R2* maps were evaluated independently by the three radiologists (S.R., M.M., C.F.). Readers were blinded to image acquisition techniques (2D versus 3D) and the reading order of R2* maps in all subjects was randomized. A motion-related artifact score using the following scale was used: 0, non-diagnostic; 1, severe artifacts, but evaluation of some relevant anatomy is possible; 2, modest

artifacts, with only mild impairment of evaluation of relevant anatomy; 3, no significant artifacts. Placental R2* measurements were obtained by drawing three ~2.4 cm^2 oval ROIs in the superior, middle and inferior regions of the placenta, separately, using T2-weighted SSFSE as anatomic references. ROIs were co-localized in 2D and 3D CSE-MRI and adjusted if required. The radiologist (M.M.) confirmed all ROI locations in the placenta.

In the repeatability study, placental R2* measurements were obtained by drawing three ~2.4 cm^2 oval ROIs in the superior, middle and inferior regions of the placenta, separately, using T2-weighted SSFSE as anatomic reference. ROIs were co-localized in all imaging series. The radiologist (M.M.) confirmed all ROI locations in the placenta. The within-technique mean difference (MD_{within}), within-technique standard deviation (SD_{within}), and coefficient of repeatability (CR) were calculated between the two repeated scans.

Data Analysis

Phantoms—Linear regression analysis (Pearson's correlation r^2 and Lin's concordance correlation coefficient ρ) and Bland-Altman analysis were used to assess the correlation and bias of both R2* and ΔB0 estimated in 2D CSE-MRI compared to the measurements in 3D CSE-MRI.

Animals—Linear regression analysis (Pearson's correlation r^2 and Lin's concordance correlation coefficient ρ) and Bland-Altman analysis were used to assess the correlation of R2*, log(R2*) and ΔB0 estimated in 2D versus 3D CSE-MRI. Moreover, a linear mixed-effects model was used to analyze the inter-animal variability of placental R2* and ΔB0 measurements. R2* measurements in 2D were modeled as a linear function of R2* measurements in 3D and the model included random effects on the slope and intercept for animal and random effects on the slope and intercept for ROI locations (i.e., in anterior or posterior placental disc). ΔB0 measurements in 2D were modeled as a linear function of ΔB0 measurements in 3D and the model included random effects on the slope and intercept for animal. Statistical significance was defined as $P \lesssim 0.05$.

Humans—In the motion assessment study, the readers' score in 2D CSE-MRI and 3D CSE-MRI were compared by using Student's t-test. Mean placental R2* of the three ROIs measured in 2D and 3D CSE-MRI were compared by using Student's t-test.

All statistical analysis was performed using Matlab (MathWorks, Natick, MA).

Results

Phantoms

Figure 1 shows the T1-weighted structural reference image (a), R2* map (b) and B0 field map (c) of a single slice in 3D CSE-MRI high SNR acquisition of four vials in one batch of the phantom. Boundary B0 measurements ΔB0 of one vial and the adjacent water are illustrated in yellow dashed oval ROIs in the zoomed-in B0 field map (d). The measurements of the other seven vials were performed analogously. Figures 1e and 1f show R2* and ΔB0 of all eight vials with varying ferumoxytol concentrations measured in the four CSE-MRI acquisitions. Both R2* and ΔB0 increase approximately linearly with increased ferumoxytol

concentrations in 2D CSE-MRI high SNR and 3D CSE-MRI high SNR, throughout the entire range of ferumoxytol concentrations. In 2D CSE-MRI and 3D CSE-MRI, R2* and ΔB0 also increase at moderate ferumoxytol concentrations (i.e., <176 μg/mL). Relative to the reference measurements from 3D CSE-MRI high SNR, bias in both R2* and ΔB0 measurements was observed in 3D CSE-MRI at high ferumoxytol concentrations (i.e., ≥ 220 μg/mL). Similarly, bias in R2* and ΔB0 measurements was observed in 2D CSE-MRI at high ferumoxytol concentrations (i.e., ≥ 176 μg/mL).

Figure 2 shows the linear regression (a1-f1) and Bland-Altman analysis (a2-f2) of R2* and ΔB0 measured in 2D CSE-MRI (a, d), 2D CSE-MRI high SNR (b, e) and 3D CSE-MRI (c, f) in comparison with the reference measured in 3D CSE-MRI high SNR in the phantom. R2* and ΔB0 measurements in all three protocols at low R2* and ΔB0 values are highly correlated with the reference, indicated by the distribution of measurements close to y=x in linear regression analysis (dashed line in a1-f1), and show low bias as indicated by the Bland-Altman analysis (a2-f2). In 2D CSE-MRI, particularly for reference R2* values below 390.0 s^{-1} (bold markers, fonts, and lines in a1, a2, d1, d2), a slope of 0.94 (r^2=0.99, ρ=0.99) in linear regression and a bias of −4.8 s^{-1} with limits of agreement of (−41.4, 31.8) s^{-1} are observed in R2* measurements, and a slope of 1.07 (r^2=1.00, ρ=0.99) and a bias of 11.4 Hz with limits of agreement of (−12.0, 34.8) Hz are observed in ΔB0 measurements. However, both R2* and ΔB0 are underestimated at high R2* and ΔB0 values, i.e.: R2*>400.0 s^{-1} and a ΔB0>300.0 Hz in 2D CSE-MRI (a, d) and a reference R2*>500.0 s^{-1} and a ΔB0>400.0 Hz in 3D CSE-MRI (c, f). Bias in both R2* and ΔB0 measurements is reduced at high R2* and ΔB0 values by increasing SNR, i.e., in 2D CSE-MRI high SNR (b, e).

Animals

One 3D CSE-MRI of an animal (Rhesus #1) at a scan time point was considered as having severe artifacts and rejected for R2* and B0 measurements by two readers (Reader-1 and Reader-3). Two additional 3D CSE-MRI acquisitions were considered as having severe artifacts by one reader (Reader-1 and Reader-3, respectively), but were accepted by the two remaining two readers, and therefore were included in the analysis. All remaining 3D CSE-MRI acquisitions, as well as all 2D CSE-MRI acquisitions in animals were confirmed as without significant artifacts by all three readers. Figure 3 shows the anatomic water images, R2* maps and B0 field maps in a pregnant rhesus macaque (Rhesus #4) acquired using 2D CSE-MRI and 3D CSE-MRI, both before (upper two rows) and immediately after ferumoxytol administration (bottom two rows). The uterine cavity and two separate placental discs are delineated by orange lines and blue lines, respectively, and the amniotic fluid is indicated by the green arrow in the anatomic images. Amniotic fluid was found to be a reliable reference tissue for boundary B0 measurements as no ferumoxytol uptake is observed, indicated by stable R2* measurements throughout multiple days. R2* and B0 field of both placental discs are elevated after ferumoxytol administration.

Example ROIs for R2* measurements and B0 measurements are shown in Supporting Information Figure S1. The linear regression analysis and Bland-Altman analysis of R2* and ΔB0 measured in 2D CSE-MRI and 3D CSE-MRI are shown in Figure 4. R2* measurements from all animals at all scan time points are consistent in 2D and 3D CSE-MRI

with a slope of 0.92 (r^2=0.97, ρ=0.98) in the linear regression on R2* (4a) and a slope of 0.90 (r^2=0.95, ρ=0.97) in the linear regression on log(R2*) (4c). The slope of the linear fit of ΔB0 between 2D and 3D CSE-MRI (4e) is close to 1 (1.05 with r^2=0.95, ρ=0.97). All correlations were statistically significant with P<0.001. The bias observed in R2* and ΔB0 is small in all animals, while variations are relatively large at high R2* and ΔB0 values, indicated by the relatively broad limits of agreement (4b, 4d, 4f).

The mixed-effects model analysis shows that the variability of both R2* (Table 2) and ΔB0 (Table 3) measured in 2D versus 3D CSE-MRI across animals, shown as the standard deviation, is large. This analysis indicates relatively large impact of measurements from individual animals, more specifically Rhesus #1, Rhesus #4 and Rhesus #11 on R2* measurements and Rhesus #5 and Rhesus #11 on ΔB0 measurements. The variability of R2* measured across placental discs (anterior and posterior placental) is small.

Humans

Preliminary Motion Assessment—Figure 5 shows the anatomic image, R2* map and B0 field map from 2D CSE-MRI and 3D CSE-MRI, respectively, acquired in two adult pregnant women (Subject #1, 20 weeks and 5 days of gestation; Subject #10, 21 weeks and 1 days of gestation). In Subject #1 (upper rows), motion artifacts are observed in both R2* and B0 field maps in 3D CSE-MRI (score of 1, 1 and 2 by Reader-1, Reader-2 and Reader-3, respectively), while there are no obvious artifacts in the co-localized slice from 2D CSE-MRI (score of 3 by all three readers). In Subject #10 (lower rows), there are no obvious motion artifacts in R2* maps and B0 field maps from both 3D CSE-MRI (score of 2, 2 and 3 by Reader-1, Reader-2 and Reader-3, respectively) and 2D CSE-MRI (score of 2, 3 and 3 by Reader-1, Reader 2 and Reader-3, respectively).

A score of 2.9±0.3, 3.0±0 and 3.0±0 for motion assessment in 2D CSE-MRI is significantly higher than a score of 1.8±0.6, 1.3±0.7, 1.9±0.6 in 3D CSE-MRI in Reader-1 (P=0.001), Reader-2 (P<0.001) and Reader-3 (P<0.001). Mean placental R2* of all ten subjects is 10.2 s^{-1} with a range of 6.7 s^{-1} to 15.9 s^{-1} measured in 2D CSE-MRI. It is not significantly (P=0.174) different from the mean placental R2* of 11.3 s^{-1} with a range of 8.3 s^{-1} to 13.2 s^{-1} measured in 3D CSE-MRI.

Preliminary Repeatability Study—In the ROIs of the seven human subjects, a MD_{within} of 0.7 s^{-1}, SD_{within} of 3.4 s^{-1}, and CR of 9.5 s^{-1} were observed in the repeated 2D CSE-MRI, as shown in Table 4. A MD_{within} of −0.2 s^{-1}, SD_{within} of 3.8 s^{-1}, and CR of 10.6 s^{-1} were observed in the repeated 3D CSE-MRI.

Discussion

In this study, we have evaluated the accuracy of R2* and B0 field measurements obtained from 2D CSE-MRI acquisitions without respiratory gating by comparing the correlation and bias to the reference 3D CSE-MRI acquisition in phantoms and pregnant rhesus macaques. High correlation and low bias of both R2* and boundary B0 field measurements in 2D CSE-MRI compared to 3D CSE-MRI were observed in a phantom over a wide range of R2* values. Additionally, high correlation and low bias were also observed in ferumoxytol-

enhanced MRI of the pregnant rhesus macaques, demonstrating the accuracy of 2D CSE-MRI in the presence of maternal respiratory motion. Further, we preliminarily evaluated motion artifacts and repeatability of 2D CSE-MRI for placental R2* mapping in pregnant women without ferumoxytol administration. The high score for motion assessment in 2D CSE-MRI showed no significant artifacts, demonstrating its motion-robustness due to the short temporal footprint for each acquired slice. Preliminary assessment indicated repeatable R2* mapping in pregnant subjects.

The study with animals under general anesthesia enables reliable imaging with 3D CSE-MRI in the absence of fetal motion, which provides reference R2* and B0 measurements. This experiment design provides a unique opportunity to perform in vivo evaluation of the accuracy of 2D CSE-MRI by comparing to the reference 3D CSE-MRI, as this reference will likely not be reliable in the presence of fetal motion.

Joint analysis of the MRI measurements for iron concentration and cell and tissue localization experiments on the animal model in this study of inflammation at the maternal-fetal interface are under separate investigation. This joint analysis will assess the feasibility of ferumoxytol-enhanced placental MRI in an inflammation model, which may potentially enable assessment of macrophage activation and localization at the maternal-fetal interface. Upon assessment of safety and regulatory approval, ferumoxytol-enhanced CSE-MRI may be applied in pregnant women to validate its potential as a non-invasive approach for identifying immune cell homing, which may enable early assessment of the developing preeclampsia.

Sixteen echo times up to 18 ms in 2D CSE-MRI in this inflammation study were optimized to capture potentially modest changes in R2* values. TR was thus relatively long, leading to ~3 seconds scan time for each slice. The temporal footprint for each slice can be further shortened by reducing the number of echo times, leading to a reduced TR. In 3D CSE-MRI, however, fewer echoes (i.e., eight echo times) were acquired in order to reduce the scan time, which was already lengthy due to the need for respiratory gating.

CSE-MRI acquisitions were performed at different field strengths for animals (at 3.0T) and humans (1.5T) in this work. The high SNR at 3.0T benefits the MRI quantification in animal studies, which also required higher spatial resolution. When the human study started, a wide-bore 1.5T scanner in our institute was preferred based on subject comfort and research availability considerations. In addition, this was our first research MRI study in pregnant humans at our institute. Therefore 1.5T was chosen for the human studies, in consideration of potential issues like specific absorption rate (SAR) for some MRI techniques applied in this human placenta study.

The SNR in 2D sequential SGRE acquisition is generally lower than SNR in 3D SGRE (12). The range of R2* and B0 field that can be measured without bias is affected by SNR, as shown in the phantom study. Thus, high SNR may need to be achieved to provide accurate R2* and B0 field estimations at high ferumoxytol concentrations especially in macrophages of the reticuloendothelial system (e.g., liver, spleen, bone marrow) where iron deposition can remain high after ferumoxytol injection (29). In macrophages outside the reticuloendothelial

system in inflammation response, however, moderate iron concentrations have been observed which can be detectable with current CSE-MRI techniques (9, 30, 31). Thus, the dynamic range of the iron concentration at macrophage homing sites of inflammation at the maternal-fetal interface is expected to be moderate, although the exact range is still unknown (and is under current investigation in our ongoing projects). Therefore, the proposed 2D CSE-MRI technique is expected to be effective for potential ferumoxytol-enhanced MRI studies of inflammation at the maternal-fetal interface.

Although the proposed boundary B0 measurements provide a measurement of magnetic susceptibility, reconstruction of magnetic susceptibility maps may be desirable. Unfortunately, quantitative susceptibility mapping requires a 3D B0 field map, which is not readily available in 2D CSE-MRI due to potential mis-registration between slices. Nevertheless, the boundary B0 measurements are feasible in 2D CSE-MRI and thus enable a magnetic susceptibility measure to assess iron concentration as demonstrated in previous works (3, 28).

This study has several limitations. First, the evaluation of 2D CSE-MRI in the presence of fetal motion is limited in animals under general anesthesia. Comprehensive repeatability studies in ferumoxytol phantoms with aperiodic motion, animals and human subjects at different gestation states are needed to further evaluate 2D CSE-MRI for R2* and B0 field mapping in placental imaging. In the presence of fetal motion, however, we expect 2D CSE-MRI to provide good image quality within slices acquired during quiescent periods without fetal motion (and possibly also with moderate motion). In addition, motion assessment needs to be performed in a large number of human subjects. Further, R2* of the whole placental discs in both animals and human subjects needs to be assessed in future studies to evaluate the spatial distribution of the iron concentration in the placenta and the placental oxygenation.

In conclusion, this study demonstrated 2D CSE-MRI as a promising technique for accurate evaluation of R2* and B0 field in the placenta without the need for respiratory bellows or navigators. Further evaluation of 2D CSE-MRI for the detection and quantification of ferumoxytol in the setting of motion is warranted. Upon successful validation, the motion-robust technique may provide a reliable approach for R2*- and B0 mapping-based evaluation of placental health in ferumoxytol-enhanced placental MRI, and BOLD-based placental functional imaging (21).

Supplementary Material

Refer to Web version on PubMed Central for supplementary material.

Acknowledgements:

The authors thank GE Healthcare who provides research support to University of Wisconsin-Madison. The authors gratefully acknowledge Colin Longhurst, MS who provided assistance with statistical anlaysis. Additionally, the authors thank AMAG Pharmaceuticals Inc. for providing ferumoxytol used in animal studies. Further, Dr. Reeder is a Romnes Faculty Fellow, and has received an award provided by the University of Wisconsin-Madison Office of the Vice Chancellor for Research and Graduate Education with funding from the Wisconsin Alumni Research Foundation.

Grant Support: National Institutes of Health (NIH); Grant numbers: U01-HD087216, R01-DK117354, R01-DK100651, K24-DK102595, and P51-OD011106.

References

1. Faas MM, Spaans F, De Vos P. Monocytes and macrophages in pregnancy and pre-eclampsia. Front Immunol 2014; 5:298. [PubMed: 25071761]
2. Bashir MR, Bhatti L, Marin D, Nelson RC. Emerging applications for ferumoxytol as a contrast agent in MRI. J Magn Reson Imaging 2015; 41(4):884–898. [PubMed: 24974785]
3. Hernando D, Cook RJ, Diamond C, Reeder SB. Magnetic susceptibility as a B0 field strength independent MRI biomarker of liver iron overload. Magn Reson Med 2013; 70(3):648–656. [PubMed: 23801540]
4. Christen T, Ni W, Qiu D, et al. High-resolution cerebral blood volume imaging in humans using the blood pool contrast agent ferumoxytol. Magn Reson Med 2013;70:705–710. [PubMed: 23001902]
5. Rivera-Rivera LA, Schubert T, Knobloch G, et al. Comparison of ferumoxytol-based cerebral blood volume estimates using quantitative R1 and R2* relaxometry. Magn Reson Med 2018;79(6):3072–3081. [PubMed: 29096054]
6. Stirrat CG, Alam SR, MacGillivray TJ, et al. Ferumoxytol-enhanced magnetic resonance imaging methodology and normal values at 1.5 and 3T. J Cardiovasc Magn Reson 2016; 18(1):p.46. [PubMed: 27465647]
7. Sharma SD, Hernando D, Horng DE, Reeder SB. Quantitative susceptibility mapping in the abdomen as an imaging biomarker of hepatic iron overload. Magn Reson Med 2015; 74(3):673–683. [PubMed: 25199788]
8. Neuwelt A, Sidhu N, Hu CA, Mlady G, Eberhardt SC, Sillerud LO. Iron-based superparamagnetic nanoparticle contrast agents for MRI of infection and inflammation. Am J Roentgenol 2015; 204(3):W302–W313. [PubMed: 25714316]
9. Gaglia JL, Harisinghani M, Aganj I, et al. Noninvasive mapping of pancreatic inflammation in recent-onset type-1 diabetes patients. Proc Natl Acad Sci. 2015;112(7):2139–44. [PubMed: 25650428]
10. Prayer D, Bruggere PC, Prayer L. Fetal MRI: techniques and protocols. Pediatr Radio 2004; 34(9):685–693.
11. Hines CD, Frydrychowicz A, Hamilton G, et al. T1 independent, T2* corrected chemical shift based fat–water separation with multi-peak fat spectral modeling is an accurate and precise measure of hepatic steatosis. J Magn Reson Imaging 2015. 2011; 33(4):873–81.
12. Utaroh Motosugi, Hernando D, Bannas P, et al. Quantification of liver fat with respiratory-gated quantitative chemical shift encoded MRI. J Magn Reson Imaging 2015; 42(5):1241–1248. [PubMed: 25828696]
13. Taviani V, Hernando D, Francois CJ, et al. Whole-heart chemical shift encoded water–fat MRI. Magn Reson Med 2014; 72(3):718–25. [PubMed: 24186810]
14. Armstrong T, Dregely I, Stemmer A, et al. Free-breathing liver fat quantification using a multiecho 3D stack-of-radial technique. Magn Reson Med 2018; 79(1):370–82. [PubMed: 28419582]
15. Armstrong T, Liu D, Martin T, et al. 3D Mapping of the Placenta During Early Gestation Using Free-Breathing Multiecho Stack-of-Radial MRI at 3T. J Magn Reson Imaging 2018 in press. doi: 10.1002/jmri.26203.
16. Pooler BD, Hernando D, Ruby JA, Ishii H, Shimakawa A, Reeder SB. Validation of a motion-robust 2D sequential technique for quantification of hepatic proton density fat fraction during free breathing. J Magn Reson 2018 in press. doi: 10.1002/jmri.26056.
17. Keraudren K, Kuklisova-Murgasova M, Kyriakopoulou V, et al. Automated fetal brain segmentation from 2D MRI slices for motion correction. NeuroImage 2014; 101:633–643. [PubMed: 25058899]
18. Levine D, Barnes PD, Sher S, et al. Fetal fast MR imaging: reproducibility, technical quality, and conspicuity of anatomy. Radiology 1998; 206(2):549–554. [PubMed: 9457211]

19. Sinding M, Peters DA, Frokjær JB, et al. Placental magnetic resonance imaging T2* measurements in normal pregnancies and in those complicated by fetal growth restriction. Ultrasound Obstet Gynecol 2016; 47:748–754. [PubMed: 26041014]
20. Huen I, Morris DM, Wright C, et al. R1 and R2 * changes in the human placenta in response to maternal oxygen challenge. Magn Reson Med 2013; 70:1427–1433. [PubMed: 23280967]
21. Schabel MC, Roberts VH, Lo JO, et al. Functional imaging of the nonhuman primate Placenta with endogenous blood oxygen level–dependent contrast. Magn Reson Med 2016;76(5):1551–62. [PubMed: 26599502]
22. Esch EV, Cline JM, Buse E, et al. Summary comparison of female reproductive system in human and the cynomolgus monkey (macaca fascicularis). Toxicol Pathol 2008;36:171S–172S.
23. Blankenship TN, Enders AC, King BF. Trophoblastic invasion and the development of uteroplacental arteries in the macaque: immunohistochemical localization of cytokeratins, desmin, type IV collagen, laminin, and fibronectin. Cell Tissue Res 1993;272:227–236. [PubMed: 7685655]
24. de Rijk EPICT, Van Esch E The macaque placenta-a mini-review. Toxicol Pathol 2008;36:108S–118S.
25. Martin CG Jr, Ramsey EM. Gross anatomy of the placenta of rhesus monkeys. Obstet Gynecol 1970;36(2):167–77. [PubMed: 4987878]
26. Ludwig KD, Fain SB, Nguyen S, et al. Perfusion of the placenta assessed using arterial spin labeling and ferumoxytol dynamic contrast enhanced magnetic resonance imaging in the rhesus macaque. Magn Reson Med 2019;81(3):1964–1978. [PubMed: 30357902]
27. Yu H, Shimakawa A, McKenzie CA, Brodsky E, Brittain JH, Reeder SB. Multiecho water-fat separation and simultaneous R2* estimation with multifrequency fat spectrum modeling. Magn Reson Med 2008; 60(5):1122–1134. [PubMed: 18956464]
28. Wang ZJ, Li S, Haselgrove JC. Magnetic resonance imaging measurement of volume magnetic susceptibility using a boundary condition. J Magn Reson 1999; 140:477–481. [PubMed: 10497053]
29. Storey P, Lim RP, Chandarana H, et al. MRI assessment of hepatic iron clearance rates after USPIO administration in healthy adults. Invest Radiol 2012;47:717–724. [PubMed: 23070094]
30. Iv M, Samgbabadi P, Holdsworth S, et al. Quantification of macrophages in high-grade gliomas by using ferumoxytol-enhanced MRI: a pilot study. Radiology 2019;290(1):198–206. 11 6:181204. [PubMed: 30398435]
31. Stirrat CG, Alam SR, MacGilivray TJ, et al. Ferumoxytol-enhanced magnetic resonance imaging assessing inflammation after myocardial infarction. Heart 2017; 103:1528–1535. [PubMed: 28642288]

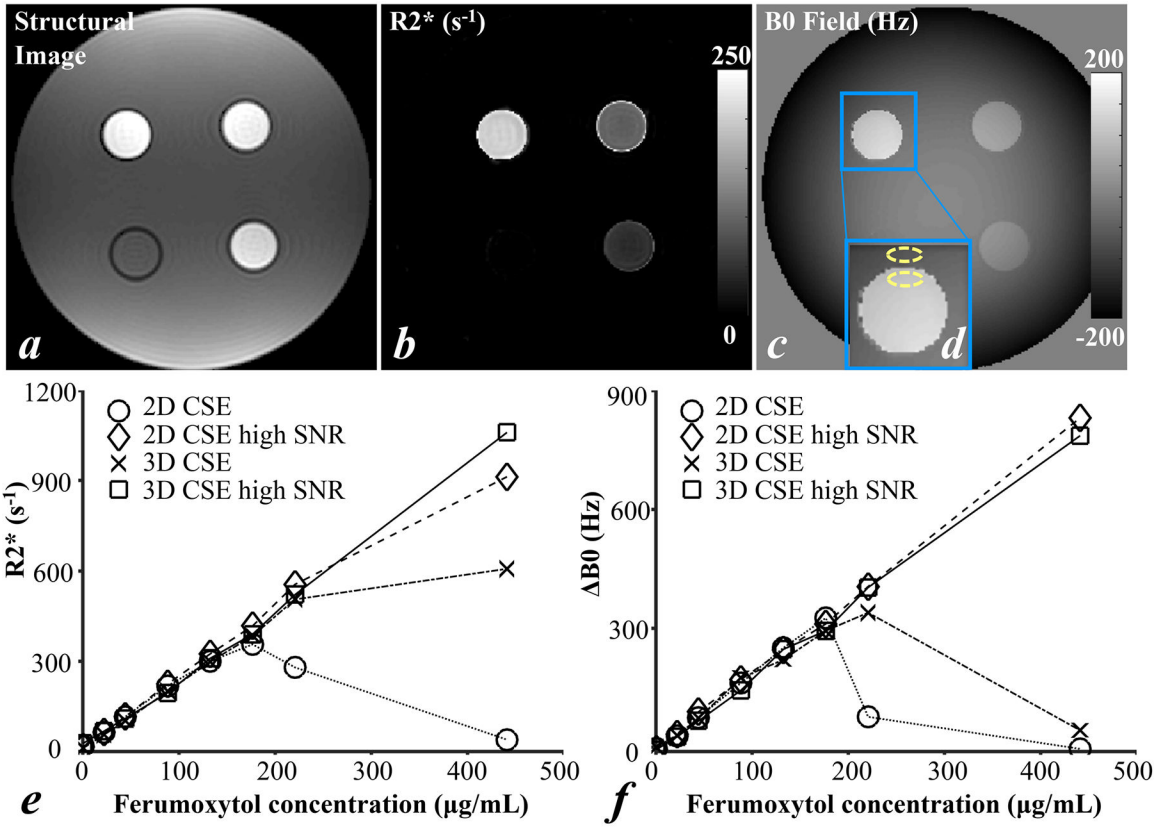

Figure 1.

T1-weighted Structural reference image (a), R2* map (b) and B0 field map (c) of a single slice in 3D CSE-MRI acquisition of four vials in one batch of the phantom scans, R2* (e) and ΔB0 (f) of all eight vials with varying ferumoxytol concentrations measured in the four CSE-MRI acquisition. An example of boundary B0 field measurement is indicated by two yellow dashed oval ROIs in the zoomed B0 field map (d).

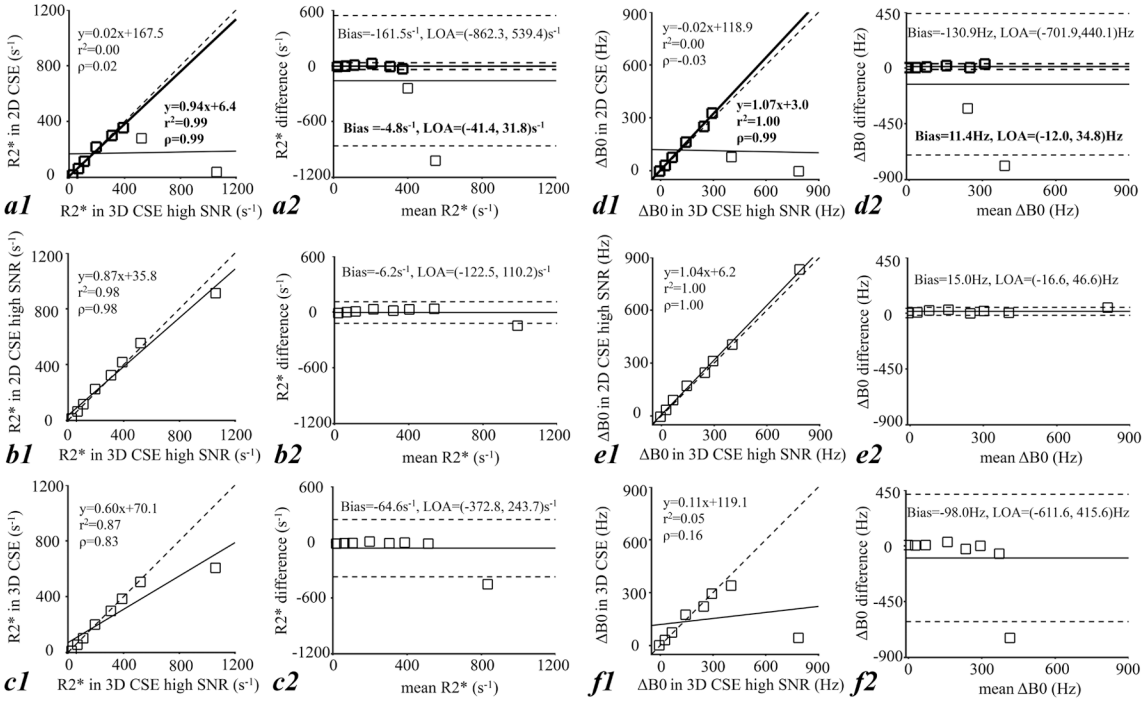

Figure 2.

Results from phantom scans: linear regression analysis (a1, f1) and Bland-Altman analysis (a2-f2) of R2* and ΔB0 measured in 2D CSE-MRI (a, d), 2D CSE-MRI high SNR (b, e), and 3D CSE-MRI (c, f) in comparison with the reference measured in 3D CSE-MRI high SNR. Small bias on both R2* and ΔB0 measurements at relatively low R2* and ΔB0 values indicates good correlation of measurements in the three CSE-MRI acquisitions and the reference CSE-MRI acquisition, while the large bias at high R2* and ΔB0 values indicated limited measurable range of each CSE-MRI acquisition. Particularly in 2D CSE-MRI, high linear correlation and small bias on both R2* and ΔB0 were observed for reference R2* values below 390.0 s^{-1} (bold markers, fonts, and lines in a1, a2, d1, d2).

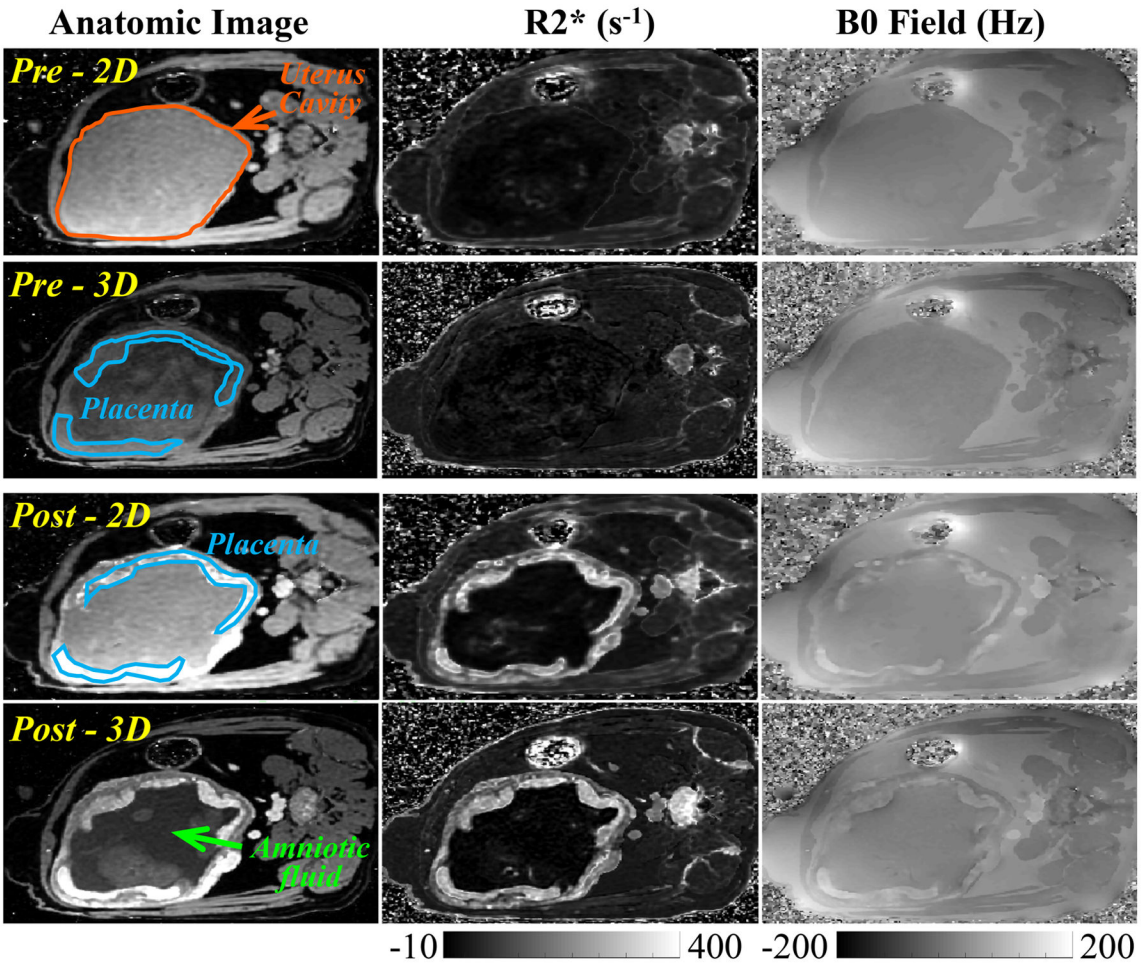

Figure 3.

Representative anatomic images, R2* maps, and B0 field maps from 2D and 3D CSE-MRI acquisitions in a pregnant rhesus macaque (Rhesus #4) at scans before (Pre) and immediately after (Post) ferumoxytol administration. Two placental discs and the uterus cavity are delineated by blue lines and orange lines, respectively. The amniotic fluid is indicated with a green arrow on the anatomic image.

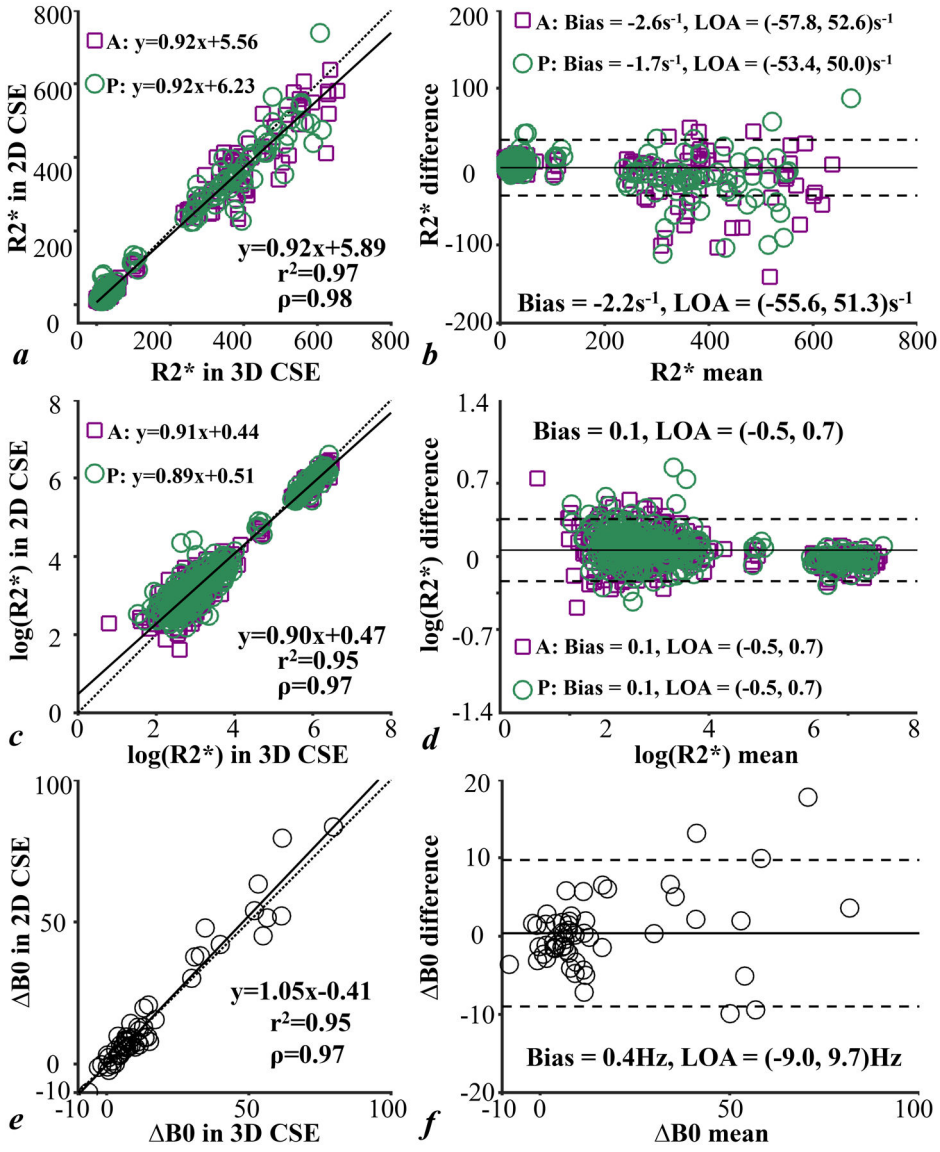

Figure 4.

Linear regression analysis (a, c, e) and Bland-Altman analysis (b, d, f) of R2*, log(R2*) and ΔB0 measured in 2D CSE-MRI in comparison with the measurements in 3D CSE-MRI of anterior placental disc, posterior placental disc and both together in animals. R2* and ΔB0 measurements are consistent in 2D and 3D CSE-MRI acquisitions.

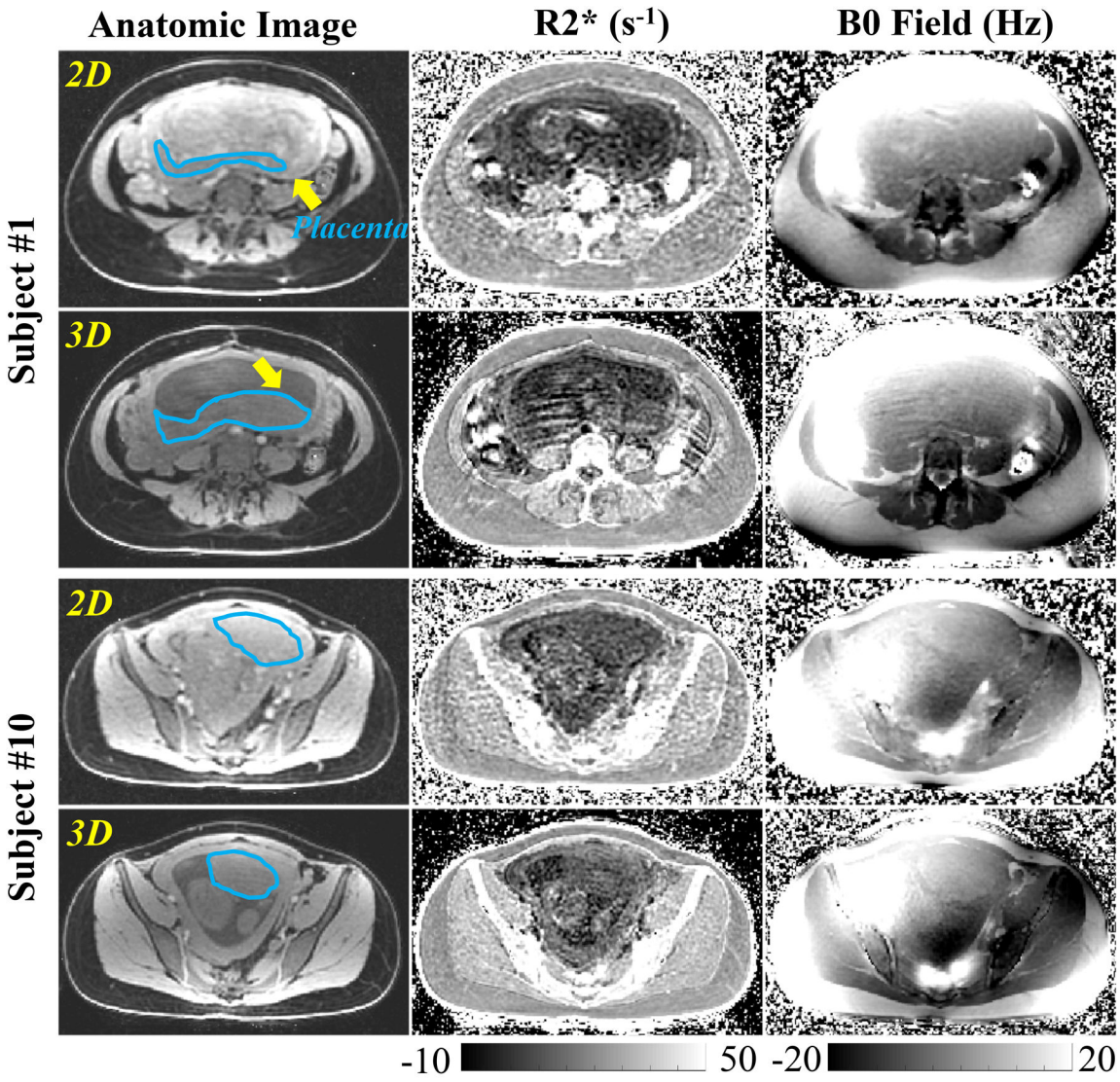

Figure 5.

Anatomic images, R2* maps, and B0 field maps of 2D and 3D CSE-MRI in two pregnant women. Motion artifacts are observed in the R2* map and B0 field map in 3D CSE-MRI of Subject #1, while no obvious artifacts are observed by the radiologist in 2D CSE-MRI. The placental disc of this subject (delineated by blue lines) was located in a different location of the maternal pelvic for 2D vs 3D CSE-MRI (see yellow arrows), suggesting the presence of fetal motion during this exam. No obvious artifacts or obvious movement of the placenta are observed by the radiologist in 3D or 2D CSE-MRI in Subject #10.

Table 1.

Scan parameters of 2D CSE-MRI and 3D CSE-MRI in the phantom and animal studies at 3.0T and the preliminary human studies at 1.5T.

	# TE	$TE_{init}/\Delta TE$ (ms)	TR (ms)	FA (°)	FOV (mm^3)	ACQ Resolution (mm^3)	NOA	ACQ BW (kHz)	PI Acceleration Phase/Slice	Scan Time (minutes)	Temporal Footprint per Slice
Phantom Study (3.0T)											
2D CSE-MRI	16	1.8/1.0	18.9	9	220×220×69 [+]	2.3×2.3×2.3 [+]	1	±100	1.5 / 1.0	1:34	3.1 seconds
2D CSE-MRI high SNR	16	1.8/1.0	18.9	9	220×220×72 [+]	2.3×2.3×3.0 [+]	4	±62.5	1.5 / 1.0	6:13	15.5 seconds
3D CSE-MRI [×]	8	1.6/1.3	12.8	9	220×220×68	1.5×1.5×1.2	1 [*]	±62.5	1.5 / 1.0	1:40	1:40 minutes
3D CSE-MRI high SNR [×]	8	1.6/1.3	12.8	9	220×220×72	1.5×1.7×8.0	1 [*]	±143	1.5 / 1.5	0:38	0:38 minutes
Animal Study (3.0T)											
2D CSE-MRI	16	1.8/1.0	18.7	9	180×160×140 [+]	1.9×1.8×3.0 [+]	1	±62.5	1.5 / 1.0	2:11	2.8 seconds
3D CSE-MRI	8	1.6/1.3	12.9	9	160×140×140	1.1×1.0×2	1 [*]	±62.5	1.5 / 1.0	4:54 [#]	4:54 minutes [#]
Human Study (1.5T)											
2D CSE-MRI	12	1.5/0.8	12.7	10	420×378×224 [+]	2.9×2.9×4.0	1	±62.5	1.5 / 1.0	2:14	2.4 seconds
3D CSE-MRI	6	1.2/2.0	13.9	9	420×378×228	2.2×2.2×3	1 [*]	±83.3	2.0 / 1.5	1:48 [#]	1:48 minutes
T2 SSFSE	1	100/0	4000	155	380×380×210	1.5×1.5×5	1	±83.3	2.0 / 1.0	2:40	2.8 seconds

[+] Contiguous slices with slice gap=0 mm;

[*] 3D corner cutting used (20% k-space reduction).

[×] No respiratory gating used in phantom study.

[#] Scan time with respiratory gating. CSE: chemical shift-encoded; FA: flip angle; FOV: field of view; ACQ: acquisition; NOA: number of averages; BW: sampling bandwidth; PI: parallel imaging; SSFSE: single-shot fast spin-echo

Table 2.

Linear mixed-effects model analysis of R2* measurements in different animals and imaging protocols.

Fixed Effects	**Estimated Change in R2* (s^{-1})**	***P* value**
Imaging Protocols		
R2* from CSE 3D	reference	
R2* from CSE 2D	Intercept: 5.70 (3.35, 8.05); Slope: 0.92 (0.88, 0.97)	<.001; <.001
Random Effects	**Standard Deviation of R2* (s^{-1})**	
Individual Animal	Intercept: 2.57 (2.01, 3.29); Slope: 0.07 (0.06, 0.10)	
ROI Location	Intercept: <0.0001; Slope: <0.0001	

Note – Data in parentheses are 95% confidence intervals. CSE: chemical shift-encoded

Table 3.

Linear mixed-effects model analysis of ΔB0 measurements in different animals and imaging protocols.

Fixed Effects	**Estimated Change in ΔB0 (Hz)**	***P* value**
Imaging Protocols		
ΔB0 from CSE 3D	reference	
ΔB0 from CSE 2D	Intercept: −1.14 (−2.33, 0.05); Slope: 1.09 (0.97, 1.20)	.060; <.001
Random Effects	**Standard Deviation of ΔB0 (Hz)**	
Individual Animal	Intercept: 0.89 (0.25, 3.17); Slope: 0.17 (0.10, 0.28)	

Note – Data in parentheses are 95% confidence intervals. CSE: chemical shift-encoded

Table 4.

Repeatability analysis for placental R2* measured in 2D and 3D CSE-MRI acquisitions in human subjects at 1.5T.

		MD_{within} (s^{-1})	SD_{within} (s^{-1})	CR (s^{-1})
2D CSE-MRI	All (N=21)	0.7	3.4	9.5
	Superior (N=7)	1.0	2.7	7.6
	Middle (N=7)	1.6	3.4	9.4
	Inferior (N=7)	−0.7	4.1	11.3
3D CSE-MRI	All (N=21)	−0.2	3.8	10.6
	Superior (N=7)	0.5	5.1	14.1
	Middle (N=7)	−0.4	2.4	6.6
	Inferior (N=7)	−0.6	4.1	11.3

Note – CSE: chemical shift-encoded. MD_{within}=within-technique mean difference. SD_{within}=within-technique standard deviation. CR=coefficient of repeatability